Elevated pore pressure and anomalously low stress in regions of low frequency earthquakes along the Nankai Trough subduction megathrust

Hiroko Kitajima[1,2] and Demian M. Saffer[1]

[1]   Recent seismic reflection and ocean bottom seismometer (OBS) studies reveal broad regions of low seismic velocity along the Nankai subduction plate boundary megathrust off-shore SW Japan. These low velocity zones (LVZ's) extend ~55 km landward from the trench, corresponding to depths of >~10 km below sea floor. Here, we estimate the in-situ pore pressure and stress state within these LVZ's by combining P-wave velocities obtained from the geophysical surveys with new well-constrained empirical relations between P-wave velocity, porosity, and effective mean stress defined by laboratory deformation tests on drill core samples of the incoming oceanic sediment. We document excess pore pressures of 17–87 MPa that extend ~55 km into the subduction zone, indicating that trapped pore fluids support ~45–91% of the overburden stress along the base of the upper plate and surrounding major fault zones. The resulting effective stresses in the LVZ are limited to ~1/3 of the values expected for non-overpressured conditions. These low effective stresses should lead to a mechanically weak and predominantly aseismic plate boundary. The region of lowest effective stress coincides with precisely located very low frequency earthquakes, providing the first quantitative evidence linking these anomalous slip events to low stress and high pore pressure. **Citation:** Kitajima, H., and D. M. Saffer (2012), Elevated pore pressure and anomalously low stress in regions of low frequency earthquakes along the Nankai Trough subduction megathrust, *Geophys. Res. Lett.*, *39*, L23301, doi:10.1029/2012GL053793.

1.   Introduction

[2]   In subduction zones, high pore pressures develop due to tectonic loading, rapid burial, and mineral dehydration [e.g., *Moore and Vrolijk*, 1992]. Pore pressure is one important control on the strength and sliding stability of faults, and on the geometry of accretionary wedges [e.g., *Davis et al.*, 1983]. Recent studies also suggest that slow slip events (SSE), very low frequency earthquakes (VLFE), and episodic tremor and slip (ETS) are linked to high pore pressure [e.g., *Ito and Obara*, 2006; *Sugioka et al.*, 2012]. However, stress and pore pressure at depth are difficult to quantify directly, and downhole measurements of in-situ stress are generally limited to a few km depth [e.g., *Zoback and Healy*, 1992]. Previous studies have estimated stress and pore pressure in subduction zones from laboratory recompression tests [e.g., *Karig*, 1990; *Morgan and Ask*, 2004], numerical modeling [e.g., *Saffer and Bekins*, 2002; *Rowe et al.*, 2012], and from seismic velocity structure by incorporating empirical relationships between acoustic velocity, porosity, and effective stress. Most of the latter have assumed a uniaxial (vertical) deformation (K_0) condition [e.g., *Bangs et al.*, 1990; *Hayward et al.*, 2003; *Tobin and Saffer*, 2009], which may be justified for underthrusting sediment beneath a mechanically weak décollement [e.g., *Byrne and Fisher*, 1990]. A small number of studies have explicitly considered the role of lateral tectonic stress above the décollement [e.g., *Flemings*, 2002; *Rowe et al.*, 2012; *Tsuji et al.*, 2008], but have lacked the necessary constraints on sediment consolidation behavior and seismic velocities under relevant stress paths [e.g., *Karig*, 1990].

[3]   Here, we quantify in-situ stresses and pore pressure within broad LVZ's in the Nankai subduction zone off-shore southwest Japan (Figure 1). We accomplish this by (1) obtaining robust and carefully calibrated relations between porosity, compressional wave velocity (Vp), and effective stress states from a suite of laboratory triaxial deformation tests on sediment core samples; and (2) combining these empirical relations with Vp obtained by previously published seismic reflection and OBS studies. We advance upon previous work by considering the effects of lateral tectonic stress, and by fully defining the in situ stress state, including the magnitudes of pore pressure and both vertical and horizontal stresses, using a well-defined and site-specific constitutive model for sediment consolidation.

2.   Geological Setting and Background

[4]   The Nankai Trough accretionary subduction system, located offshore southwest Japan, is formed by the subduction of the Philippine Sea plate beneath the Eurasian plate at ~4–6.5 cm/yr (Figure 1) [*Miyazaki and Heki*, 2001]. Along the Integrated Ocean Drilling Program (IODP) Nankai Trough Seismogenic Zone Experiment (NanTroSEIZE) transect off-shore the Kii Peninsula, a P-wave velocity model obtained from prestack depth migration (PSDM) of 3-D seismic reflection data documents a broad zone of low seismic velocity (LVZ) in the outer subduction zone (Figure 1) [*Park et al.*, 2010]. This LVZ is developed at 2–4 km below sea floor and ~13–30 km from the trench (Figure 1b), and extends >120 km along strike [*Bangs et al.*, 2009; *Park et al.*, 2010]. Recent analysis of OBS data also documents this LVZ, and shows that anomalously low seismic velocities persist to ~10 km below sea floor and ~55 km from the trench [*Kamei*

---

[1]Department of Geosciences, Pennsylvania State University, University Park, Pennsylvania, USA.
[2]Now at Geological Survey of Japan, National Institute of Advanced Industrial Science and Technology, Tsukuba, Japan.

Corresponding author: H. Kitajima, Geological Survey of Japan, National Institute of Advanced Industrial Science and Technology, Tsukuba, Ibaraki 305-8567, Japan. (h-kitajima@aist.go.jp)
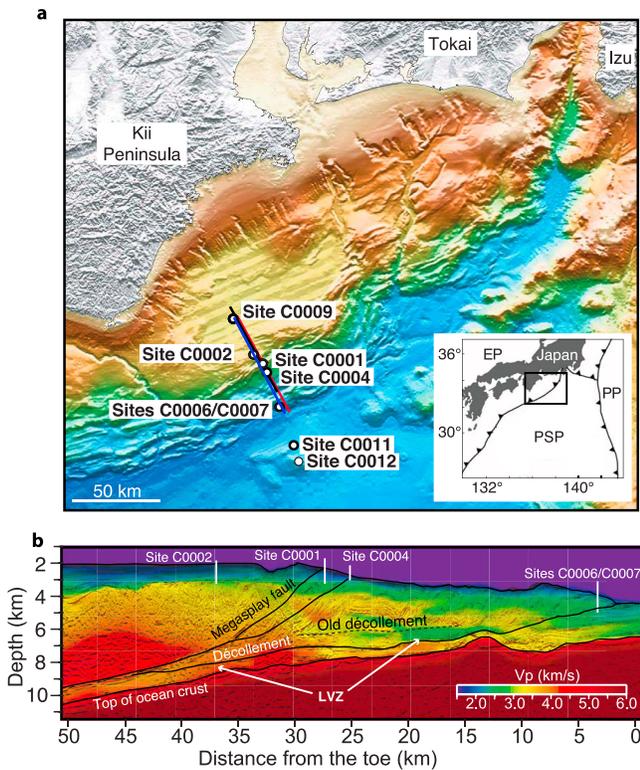
Figure 1. (a) Map of the study area (modified from *Underwood et al.* [2010]), showing locations of in-lines (IL) 2682 (red) and 2535 (blue; shown by *Park et al.* [2010]) from 3-D seismic survey, and the OBS transect used by *Kamei et al.* [2012] (black). The seismic and OBS survey lines are separated by less than ~3 km. The black box in the inset figure indicates the location of the study area. The abbreviations in the inset figure indicate tectonic plates; PSP: Philippine Sea Plate, EP: Eurasian Plate, and PP: Pacific Plate. (b) Cross section of PSDM-derived Vp along IL2535 showing major structures (after *Park et al.* [2010] and *Moore et al.* [2009]). Low P-wave velocity zones (LVZ) are observed above the active décollement between ~13–30 km from the trench, and beneath the megasplay from ~30–55 km.

et al., 2012], beneath a highly reflective region of the "megasplay", a major out of sequence thrust splay fault in the outer wedge [*Bangs et al.*, 2009] (Figure 1b). Based on the seismic interpretation of *Moore et al.* [2009], the shallower LVZ lies above the active décollement but beneath an older décollement, whereas the deeper LVZ is located beneath the megasplay near where it soles into the active décollement (Figure 1b). Because these LVZs are developed in sediments bounding the major faults in the outer forearc, and lie near the inferred updip termination of coseismic slip in the most recent great earthquake at the margin (1944 Tonankai Mw 8.2), their properties hold important implications for fault strength and slip behavior in the plate boundary system.

[5] Seismic reflection surveys and drilling at oceanic reference boreholes C0011 and C0012 indicate that along this transect the incoming sediment section is ~1000 m thick, and

includes upper-, middle-, and lower- Shikoku Basin facies, volcaniclastic-rich facies, and pelagic facies [*Moore et al.*, 2009; *Underwood et al.*, 2010]. The mudstones within the Shikoku Basin facies units are generally clay-rich (~50–60 wt%). The upper Shikoku Basin and overlying trench wedge sediments have been accreted at a frontal thrust, and the mud- and clay-rich units below this comprise the lower accretionary wedge and underthrusting package. For our experiments, we use lower Shikoku Basin (LSB) mudstone sampled from 493 m below sea floor at IODP Site C0011 (Figure 1). The observations that: (1) laboratory consolidation behavior is consistent between different mudstone core samples from the Shikoku Basin facies; (2) deformation behavior in individual laboratory tests is highly reproducible; and (3) our laboratory-defined consolidation trend matches that observed in the field (H. Kitajima and D. M. Saffer, unpublished data, 2011) all indicate that our data provide robust and representative measure of consolidation behavior for the Shikoku Basin facies mudstones.

3. Constitutive Relationships for Vp, Porosity, and Effective Stress

[6] We conducted a suite of triaxial deformation experiments to measure consolidation behavior and Vp as a function of mean and differential stress conditions, at effective axial stress (σ'_v) and effective confining pressures (P'_c) up to 70 MPa, equivalent to the overburden stress at ~5 km depth under drained conditions (hydrostatic pore pressure). (Figure S1 in the auxiliary material).[1] We define the stress paths for our experiments in terms of effective mean stress (p') and differential stress (q), which are related to the effective principal stresses, σ'_1, σ'_2, and σ'_3, (σ'_v and P'_c in our triaxial experiments) by:

$$p' = (\sigma'_1 + \sigma'_2 + \sigma'_3)/3 = (\sigma'_v + 2P'_c)/3$$

and

$$q = \sqrt{\left((\sigma'_1 - \sigma'_2)^2 + (\sigma'_2 - \sigma'_3)^2 + (\sigma'_1 - \sigma'_3)^2\right)/2} = \sigma'_v - P'_c.$$

The stress paths we explored include (1) triaxial compression ($q/p' = 1$), (2) triaxial extension ($q/p' = -1$), (3) triaxial compression under a condition of uniaxial strain (K_0), and (4) triaxial extension under a condition of radial strain ($1/K_0$).

[7] On the basis of soil mechanics theory, shear failure of a sediment or soil can be described by a critical state, at which yielding occurs by pervasive shearing without any changes in stress and volume [e.g., *Roscoe et al.*, 1958]. The critical state condition is represented as a straight line in q-p' space, and also defines a boundary between brittle and ductile deformation. We consider stress paths (1) and (2) (described by $q/p' = \pm 1$) to map the critical state line (CSL) for LSB mudstones, because we observed shear failure during an experiment following stress path (2), and because previous experiments on similar sediments define a CSL of $q/p' = 0.75$–1.3 [*Kitajima et al.*, 2012; *Karig*, 1990].

[8] The Vp-porosity-p' relationships defined by our experimental data are shown in Figure 2. The Vp-porosity trend is highly consistent with shipboard data for LSB sediments from
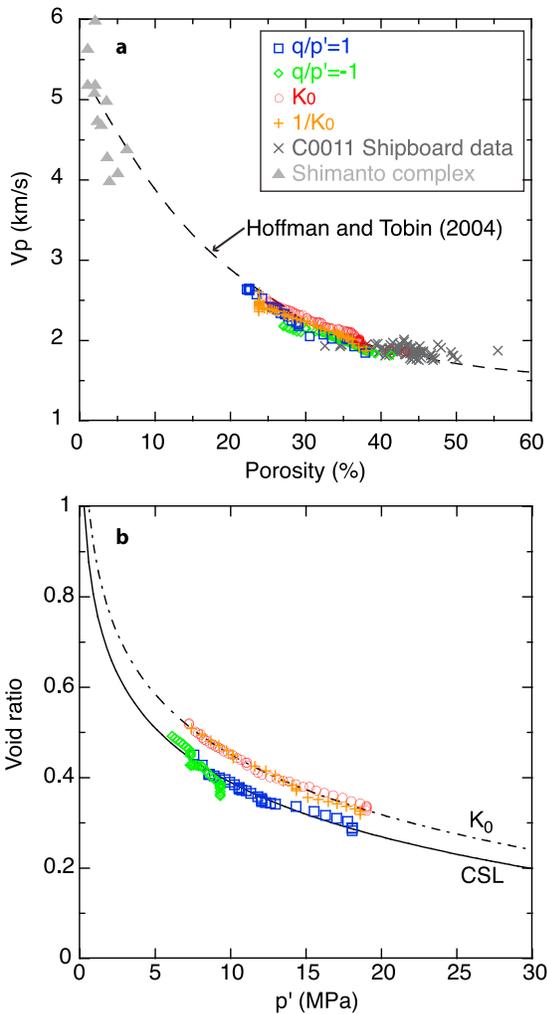
Figure 2. Experimental results, showing relationships between (a) Vp-porosity, and (b) void ratio-p', for the different stress paths (blue = triaxial compression ($q/p' = 1$); green = triaxial extension ($q/p' = -1$); red = uniaxial strain (K_0); and orange = radial strain ($1/K_0$)). Shipboard measurements for the LSB at Site C0011 [*Expedition 322 Scientists*, 2010] (gray crosses) and laboratory measurements for shales from the Shimanto accretionary complex [*Tsuji et al.*, 2008] (gray triangles) are also shown. Dashed curve in Figure 2a shows the Vp-porosity relation derived by *Hoffman and Tobin* [2004] for LSB sediment. The dot-dashed and dashed curves in Figure 2b show log-linear relations between void ratio and p' for critical state ($e = 0.79 - 0.40 \log p'$) and uniaxial/radial strain deformation ($e = 0.89 - 0.44 \log p'$), respectively.

Site C0011 [*Expedition 322 Scientists*, 2010], and with previous laboratory measurements on outcrop samples of shales from the exhumed Shimanto accretionary complex [*Tsuji et al.*, 2006] (Figure 2a). The three datasets are fit well by a Vp-porosity function derived by *Hoffman and Tobin* [2004] for LSB facies mudstones sampled by drilling ~150 km to the southwest, over a range of porosity from >50% to <5%. While the Vp-porosity relation is independent of stress path, porosity (ϕ) (or void ratio; $e = \phi/(1 - \phi)$) depends on both mean and differential stresses, consistent with the critical state
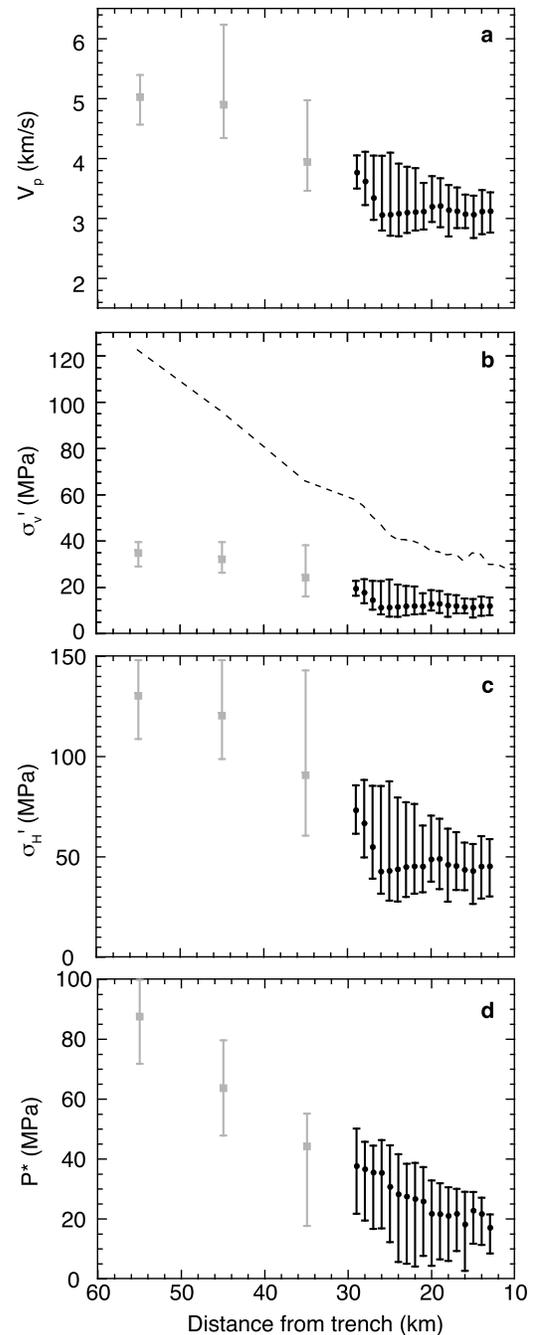
Figure 3. Values of (a) Vp, (b) σ'_v, (c) σ'_H, and (d) P^* in the LVZ with distance from the trench, computed from Vp extracted from the 3-D seismic data every 1 km and at 5 m depth intervals along IL2682 at 13–30 km from the trench (black) and the OBS survey at 35, 45, and 55 km from the trench (gray). The black dots are depth-averaged values, and the vertical bars reflect the minimum and maximum values within the LVZ at each distance from the trench. The dashed line in Figure 3b indicates the expected depth-averaged effective vertical stress for drained conditions. The uncertainty in the Vp-porosity-p' transform (~5%) and in PSDM- and OBS-derived values of Vp (~5%) results in propagated errors of ~15% in σ'_H, σ'_v, and P^*, and ~10% in λ^*.
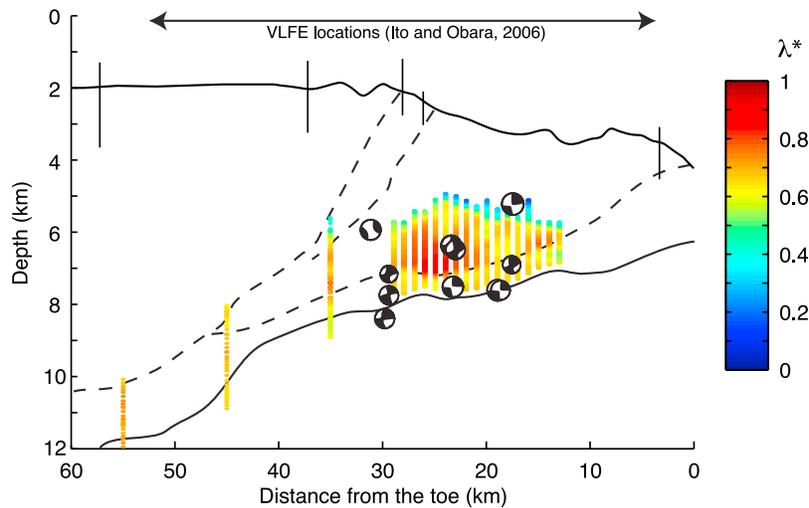
Figure 4. Distribution of λ^* in the LVZ for the case where $\sigma'_H > \sigma'_h > \sigma'_v$. The beach balls represent moment tensor solutions for VLF earthquakes reported by *Sugioka et al.* [2012]. The distribution of VLF earthquakes reported by *Ito and Obara* [2006] is also shown (top).

soil mechanics model, in which increased shear stress leads to enhanced volume loss at a given effective mean stress, but follows a log-linear trend parallel to that for uniaxial consolidation (Figure 2) [*Roscoe et al.*, 1958].

4. Estimation of In Situ Stresses and Pore Pressure in the LVZ

[9] By combining our experimentally defined Vp-porosity-p' relationships (Figure 2) with Vp values extracted from seismic reflection and OBS data, we compute porosity, and mean effective stress (p') from Vp values, under the assumption that stresses in the accretionary wedge (and in the LVZ) reflect a critical state under lateral compression. This assumption is consistent with observed active thrust faulting [e.g., *Moore et al.* 2009], fault downstepping and duplex formation in the outer accretionary wedge that indicate a laterally compressive stress state [*Byrne and Fisher*, 1990], and is analogous to the widely-held idea that accretionary wedges are characterized by pervasive horizontal compressive failure [e.g., *Davis et al.*, 1983]. To then predict σ'_H and σ'_v from the mean effective stress, the role of intermediate principal stress (σ'_h in a thrusting environment) must also be defined. We consider three scenarios: (1) $\sigma'_H = \sigma'_h > \sigma'_v$, (2) $\sigma'_H > \sigma'_h > \sigma'_v$, $\sigma'_h = (\sigma'_H + \sigma'_v)/2$, and (3) $\sigma'_H > \sigma'_h = \sigma'_v$. Here, we report results for case (2), in which σ'_H and σ'_v at the critical state condition are given by: $\sigma'_H = 1.58\ p'$, and $\sigma'_v = 0.42\ p'$ (see Figure S2 for other scenarios). We then evaluate pore pressure in the LVZ from the computed value of σ'_v; because the total overburden stress (σ_{v0}) can be estimated from bulk density data, and hydrostatic pore pressure (P_{p_hydro}) at a given depth is known, the excess pore pressure (P^*) and pore pressure ratio λ^* are given simply by $P^* = \sigma'_{v\_hydro} - \sigma'_v$ and $\lambda^* = P^* / \sigma'_{v\_hydro}$, where $\sigma'_{v\_hydro} = \sigma_{v0} - P_{p\_hydro}$.

[10] Within the LVZ, the depth-averaged mean effective stress increases from 28 MPa at 13 km from the trench, to 83 MPa at 29 km. Computed values of σ'_H increase from 43–130 MPa, σ'_v from 12–35 MPa, and P^* from 17–87 MPa over this region (Figure 3). These excess pressures

correspond to depth-averaged pore pressure ratios, λ^* ranging from 0.51–0.77, with a maximum value located 25 km from the trench (Figure 4). Comparison of P^* to σ_{v0} indicates that pore fluids support 45–91% of the overburden stress along the base of the upper plate over the outermost 55 km of the forearc. These poorly drained conditions reflect a combination of rapid tectonic loading and low sediment permeability [e.g., *Saffer and Bekins*, 2002; *Rowe et al.*, 2012]. The magnitudes of σ'_H and σ'_v we report are less than half those expected for fully drained conditions, and illustrate that elevated pore pressure allows sediment failure within a zone of anomalously low stress surrounding and beneath the megasplay and décollement (Figures 3b and 3c).

[11] The values of P^* we report should be considered an upper bound; if the sediments are not at critical state, mean stress (p') would be higher at a given Vp (and porosity), and pore pressure correspondingly lower. On the other hand, thermally enhanced consolidation or secondary compression would lead to lower values of porosity at a given mean stress, and thus result in higher excess pore pressures than we report. However, the fact that porosity-stress and Vp-porosity trends are consistent across a wide range of porosities, and for mudstones and shales subjected to a wide range of burial and loading in the natural subduction system (Figure 2) [*Tobin and Saffer*, 2009], suggests that to first order, these effects are not significant. Interestingly, if the assumption of uniaxial loading is applied, as has been assumed in some previous studies, we predict sub-hydrostatic pore pressures. This suggests that differential stress is important, and pressure and stress estimation in the region above and in the near field of the plate boundary fault (décollement) and splay fault cannot be approached by considering simple burial loading [e.g., *Bangs et al.*, 1990; *Hayward et al.*, 2003].

5. Implications for Drainage and Fault Slip Behavior

[12] It is not clear that the broad LVZ is connected at all depths, and the spatial distribution of both low velocity and elevated pore pressure appears to be heterogeneous (Figure 4).

The highest pore pressure is localized at ∼25 km from the trench and 4.5 km below sea floor in the outer wedge; pore pressure in the underthrust sediments at 30–55 km from the trench is uniformly high, although the pore pressure ratios are not as high as in the outer wedge. The spatial variability in estimated pore pressure likely reflects the combined effects of mechanical loading, mineral dehydration at temperatures of ∼60–120°C, and heterogeneous drainage along faults in the outer wedge and along the décollement.

[13] The location of VLFEs observed within and beneath the outer accretionary prism [*Ito and Obara*, 2006; *Sugioka et al.*, 2012] coincides closely with the region of lowest effective stress (Figures 3b and 4). Although elevated pore pressure has been proposed as one mechanism explaining the small stress drops and low frequency content of VLFE and slow slip events [e.g., *Ito and Obara*, 2006], we provide the first quantitative evidence to support this idea. Our results imply that the plate boundary system is both over-pressured and mechanically weak, and less likely to nucleate large earthquakes, in the outer ∼50 km of the forearc [e.g., *Scholz*, 1998]. High pore pressure has also been linked to slow rupture propagation and large seafloor uplift near the trench, and therefore may be important in controlling the extent of shallow slip and tsunamigenesis along the mega-thrust [*Ma*, 2012; *Sugioka et al.*, 2012].

References

Bangs, N. L., G. K. Westbrook, J. Ladd, and P. Buhl (1990), Seismic velocities from the Barbados Ridge complex: Indicators of high pore fluid pressures in an accretionary complex, *J. Geophys. Res.*, *95*(B6), 8767–8782, doi:10.1029/JB095iB06p08767.

Bangs, N. L. B., et al. (2009), Broad, weak regions of the Nankai Mega-thrust and implications for shallow coseismic slip, *Earth Planet. Sci. Lett.*, *284*, 44–49, doi:10.1016/j.epsl.2009.04.026.

Byrne, T., and D. Fisher (1990), Evidence for a weak and overpressured décollement beneath sediment-dominated accretionary prisms, *J. Geophys. Res.*, *95*(B6), 9081–9097, doi:10.1029/JB095iB06p09081.

Davis, D. M., J. Suppe, and F. A. Dahlen (1983), The mechanics of fold-and thrust belts, *J. Geophys. Res.*, *88*(B2), 1153–1172, doi:10.1029/JB088iB02p01153.

Expedition 322 Scientists (2010), Site C0011. In Saito, S., Underwood, M.B., Kubo, Y., and the Expedition 322 Scientists, Proc. IODP, 322: Tokyo Integrated Ocean Drilling Program Management International, Inc., Washington, DC, doi:10.2204/iodp.proc.322.104.2010.

Flemings, P. B. (2002), Overpressures above the décollement at Nankai: ODP Sites 808 and 1174, *Eos Trans. AGU*, *83*(47), Fall Meet. Suppl., Abstract H22E-08.

Hayward, N., G. K. Westbrook, and S. Peacock (2003), Seismic velocity, anisotropy, and fluid pressure in the Barbados accretionary wedge from an offset vertical seismic profile with seabed sources, *J. Geophys. Res.*, *108*(B11), 2515, doi:10.1029/2001JB001638.

Hoffman, N. W., and H. J. Tobin (2004), An empirical relationship between velocity and porosity for underthrust sediments in the Nankai Trough accretionary prism, *Proc. Ocean Drill. Program Sci. Results*, *190/196*, 1–23.

Ito, Y., and K. Obara (2006), Dynamic deformation of the accretionary prism excites very low frequency earthquakes, *Geophys. Res. Lett.*, *33*, L02311, doi:10.1029/2005GL025270.

Kamei, R., R. G. Pratt, and T. Tsuji (2012), Waveform tomography imaging of a megasplay fault system in the seismogenic Nankai subduction zone, *Earth Planet. Sci. Lett.*, *317–318*, 343–353, doi:10.1016/j.epsl.2011.10.042.

Karig, D. E. (1990), Experimental and observational constraints on the mechanical behaviour in the toes of accretionary prisms, in *Deformation Mechanisms, Rheology and Tectonics*, Geol. Soc. Spec. Publ. London, vol. 54, edited by R. J. Knipe and E. J. Rutter, pp. 383–393, Geol. Soc., London.

Kitajima, H., F. M. Chester, and G. Biscontin (2012), Mechanical and hydraulic properties of Nankai accretionary prism sediments: Effect of stress path, *Geochem. Geophys. Geosyst.*, *13*, Q0AD27, doi:10.1029/2012GC004124.

Ma, S. (2012), A self-consistent mechanism for slow dynamic deformation and tsunami generation for earthquakes in the shallow subduction zone, *Geophys. Res. Lett.*, *39*, L11310, doi:10.1029/2012GL051854.

Miyazaki, S., and K. Heki (2001), Crustal velocity field of southwest Japan: subduction and arc-arc collision, *J. Geophys. Res.*, *106*, 4305–4326, doi:10.1029/2000JB900312.

Moore, J. C., and P. Vrolijk (1992), Fluids in accretionary prisms, *Rev. Geophys.*, *30*(2), 113–135, doi:10.1029/92RG00201.

Moore, G. F., et al. (2009), Structural and seismic stratigraphic framework of the NanTroSEIZE Stage 1 transect, in *NanTroSEIZE Project Stage 1*, Proc. Integrated Ocean Drill. Program, 314/315/316, doi:10.2204/iodp.proc.314315316.102.2009.

Morgan, J. K., and M. V. S. Ask (2004), Consolidation state and strength of underthrust sediments and evolution of the décollement at the Nankai accretionary margin: Results of uniaxial reconsolidation experiments, *J. Geophys. Res.*, *109*, B03102, doi:10.1029/2002JB002335.

Park, J.-O., et al. (2010), A low-velocity zone with weak reflectivity along the Nankai subduction zone, *Geology*, *38*, 283–286, doi:10.1130/G30205.1.

Roscoe, K. H., A. N. Schofield, and M. A. Wroth (1958), On the yielding of soils, *Geotechnique*, *8*, 22–53, doi:10.1680/geot.1958.8.1.22.

Rowe, K. T., E. J. Screaton, and S. Ge (2012), Coupled fluid flow and deformation modeling of the frontal thrust region of the Kumano Basin transect, Japan: Implications for fluid pressures and decollement down-stepping, *Geochem. Geophys. Geosyst.*, *13*, Q0AD23, doi:10.1029/2011GC003861.

Saffer, D. M., and B. A. Bekins (2002), Hydrologic controls on the mechanics and morphology of accretionary wedges and thrust belts, *Geology*, *30*, 271–274, doi:10.1130/0091-7613(2002)030<0271:HCOTMA>2.0.CO;2.

Scholz, C. (1998), Earthquakes and friction laws, *Nature*, *391*, 37–42, doi:10.1038/34097.

Sugioka, H., T. Okamoto, T. Nakamura, Y. Ishihara, A. Ito, K. Obana, M. Kinoshita, K. Nakahigashi, M. Shinohara, and Y. Fukao (2012), Tsunamigenic potential of the shallow subduction plate boundary inferred from slow seismic slip, *Nat. Geosci.*, *5*, 414–418, doi:10.1038/ngeo1466.

Tobin, H. J., and D. M. Saffer (2009), Elevated fluid pressure and extreme mechanical weakness of a plate boundary thrust, Nankai Trough subduction zone, *Geology*, *37*, 679–682, doi:10.1130/G25752A.1.

Tsuji, T., G. Kimura, S. Okamoto, F. Kono, H. Mochinaga, T. Saeki, and H. Tokuyama (2006), Modern and ancient seismogenic out-of-sequence thrusts in the Nankai accretionary prism: Comparison of laboratory-derived physical properties and seismic reflection data, *Geophys. Res. Lett.*, *33*, L18309, doi:10.1029/2006GL027025.

Tsuji, T., H. Tokuyama, P. Costa Pisani, and G. Moore (2008), Effective stress and pore pressure in the Nankai accretionary prism off the Muroto Peninsula, southwestern Japan, *J. Geophys. Res.*, *113*, B11401, doi:10.1029/2007JB005002.

Underwood, M. B., S. Saito, Y. Kubo, and the Expedition 322 Scientists (2010) Expedition 322 summary. In Saito, S., Underwood, M.B., Kubo, Y., and the Expedition 322 Scientists, Proc. IODP, 322: Tokyo Integrated Ocean Drilling Program Management International, Inc., Washington, DC, doi:10.2204/ iodp.proc.322.101.2010.

Zoback, M. D., and J. H. Healy (1992), In situ stress measurements to 3.5 km depth in the Cajon Pass Scientific Research Borehole: Implications for the mechanics of crustal faulting, *J. Geophys. Res.*, *97*(B4), 5039–5057, doi:10.1029/91JB02175.